www.vbripress.com/aml, DOI: 10.5185/amlett.2016.6233 Published online by the VBRI Press in 2016

Effect of Sr-substitution on structural, dielectric and impedance characteristics of MPB-PZT

Patri Tirupathi[1], Anil Tejomurthula[2], Nawnit Kumar[3], Mukul Pastor[4]*, R. N. P. Choudhary[5]

[1]*Department of Physics, Rajiv Gandhi University of knowledge Technologies, RK Valley 516330, India*
[2]*Department of Metallurgical & Materials Engineering, Rajiv Gandhi University of Knowledge Technologies, RK Valley 516330, India*
[3]*Department of Physics, Indian Institute of Technology, Kharagpur 721302, India*
[4]*Department of Physics, Bundelkhand University, Jhansi (U.P.) 284002, India*
[5]*Department of Physics, Institute of Technical Education and Research SOA University, Bhubaneswar 751 030, India*

*Corresponding author. E-mail: mukul.ptr@gmail.com

Received: 15 September 2015, Revised: 06 December 2015 and Accepted: 22 May 2016

ABSTRACT

The polycrystalline sample of Sr-modified $Pb(Zr_{0.5}Ti_{0.5})O_3$ (i.e. $Pb_{1-x}Sr_x(Zr_{0.5}Ti_{0.5})O_3$ (x = 0.05-0.15)) ceramics were synthesized (close to morph-tropic phase boundary) by a cost effective (solid state reaction) method. Detailed investigation of structural phase transition was carried out using room temperature X-ray diffraction data adopting Rietveld refinement technique. The coexistence of two crystal phases (i.e., tetragonal (P4mm) and rhombohedral (R3c) for x = 0.05, and single tetragonal (P4mm) phase for x = 0.1, 0.15) were observed. Elemental analysis, grain shape and size distribution were studied using scanning electron microscope. The decrease in grain size on increasing Sr^{2+} concentration was also observed. Detailed analysis of temperature and frequency dependence of dielectric exhibits the increase in dielectric permittivity as function of Sr^{2+} concentration at room temperature. Beside this, the greatly reduced Curie (T_C) temperature and broadening of dielectric maxima as function of increasing Sr^{2+} concentration in PZT was observed. The multiple relaxation processes associated with grain, grain boundaries and interfacial polarization was noted for x=0.05 and x=0.10 to analyze the Nyquist plots. The dominant of grain boundary resistance with increasing in dopent concentration x=0.15 was observed. Copyright © 2016 VBRI Press.

Keywords: Polycrystalline; dielectric permittivity; rietveld refinement technique.

Introduction

$Pb(Zr_{1-x}Ti_x)O_3$ (PZT), in the form of single crystal, bulk as well as thin films, has extensively been studied owing to its large dielectric permittivity and giant piezoelectric constant for sensors, actuator, piezoelectric transformers and FeRAM applications [**1**-**3**]. Though PZT solid solutions in different Zr/Ti ratios have attracted lots of attention, (53/47) ratio (referred as morphotropic phase boundary (MPB)) has received special attention [**4**, **5**] for advanced technology. The MPB is an almost temperature independent phase boundary, where it divides two ferroelectric phases (*viz.* the tetragonal and rhombohedral) of crystal structure. The PZT near MPB displays exceptionally high piezoelectric parameters (strain coefficient d_{33}, electromechanical coupling coefficient k_p, and the mechanical quality factor Q_m and ferroelectric polarization [**6**, **7**]). In view of this, researchers have carried out considerable amount of work on dielectric and ferroelectric properties of PZT solid solutions near at MPB region. In addition to this, there are several reports on doping of rare-earth elements and divalent cations (Ba^{2+}, Sr^{2+}, Ca^{2+}) at the Pb-site in PZT near MPB region [**8**-**13**]. Among all the reports available, a large modulation in some physical properties has been observed in Sr^{2+}-doped PZT (PSZT) materials, a few of them are discussed below [**14**-**16**]. It is found that PSZT undergoes a diffuse type ferroelectric phase transition, and the diffusivity in dielectric peaks increases with increasing in Sr^{2+} concentration. This allows the PSZT materials to be used in a wide variety of devices [**14**]. In addition to, Nasar *et al.* [**15**] reported the structural change from tetragonal ferroelectric phase to tetragonal and rhombohedral ferroelectric phases (MPB) in this material**.** To study the relax or ferroelectric material near to MPB region can be used for pyroelectric and piezoelectric sensors, infrared detectors, medical imaging, and future piezoelectric transformers. Along with these materials can be used as nonvolatile random-access memories (NVRAMs) applications [**6**, **7**].

Even if considerable amount of work has been carried out on PSZT (with Zr/Ti :: 0.53/0.47), no report is available on the systematic studies of Sr^{2+} doped PZT with Zr/Ti = 0.5/0.50. This particular composition has been selected due to its proximity to MPB. Some preliminary work on structural and dielectric properties of $Pb_{0.95}Sr_{0.05}(Zr_{0.5}Ti_{0.5})O_3$ have also been reported in our recently published paper [**17**]. In the present work, a series of Sr^{2+}-doped PZT (0.50/0.50) ceramic were synthesized by a conventional high-temperature solid- state reaction method. Detailed analysis on structural phase transition was carried by Rietveld refinement method. Along with microstructural, temperature and frequency dependence of dielectric and impedance studies also presented.

Experimental

The polycrystalline samples of $Pb_{1-x}Sr_x(Zr_{0.5}Ti_{0.5})O_3$ (x= 0.05, 0.10 and 0.15) were prepared by a high-temperature solid-state reaction technique using high - purity (≥ 99.9%) ingredients: $SrCO_3$, ZrO_2, PbO, and TiO_2 in stoichiometric amount with 3% excess PbO to compensate the lead loss at elevated temperatures and mixed thoroughly in an agate-mortar in a wet condition (methanol) for 4 h. The mixtures were then calcined in a closed alumina crucible. The process of grinding and calcinations was repeated several times to optimize the calcinations temperature. The optimized calcinations temperature was 1150 °C. The formation of perovskite phase was confirmed by X-ray diffraction (XRD) technique using an X-ray powder diffractometer (PHILIPS, PW3373 XPERT-PRO). Finally, the calcined powders were used to make cylindrical pellets of diameter 12 mm and thickness 1 – 2 mm under a hydrostatic pressure of about 12 $x10^6$ N/m^2 using a hydraulic press. Polyvinyl alcohol (PVA) was used as binder which was burnt out during the high temperature sintering process. The pellets were sintered in a covered alumina crucible in air atmosphere for 6 h at 1200 °C. Electrical measurements was carried out in a wide temperature range (25 ≤ *T*≤ 500 °C) using a computer controlled phase sensitive multimeter (PSM-N4L 1735). The hysteresis loops of the poled samples were obtained using workstation of loop tracer, (M/S Radiant Technology Inc, USA).

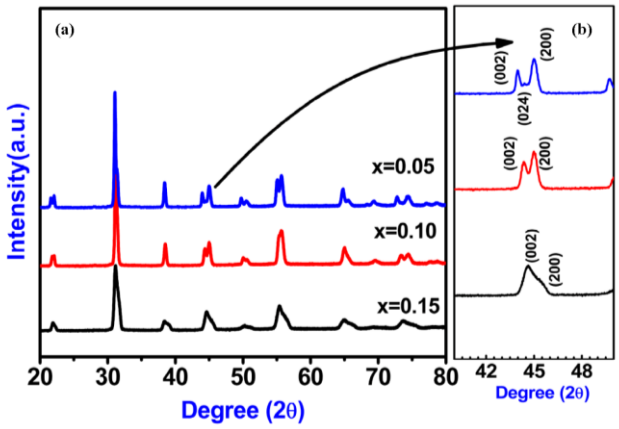

Fig. 1. (a) Evolution of X-ray diffraction Pb_{1-x} Sr_x $(Zr_{0.5}T_{0.5})O_3$ (x=0.05, 0.10 and 0.15) ceramic. (b) magnified view in the region of $42^{\circ} \leq 2\theta \leq 48^{\circ}$.

Results and discussion

Structural studies

Fig. 1(a) shows the room temperature X-ray diffraction (XRD) pattern of $Pb_{1-x}Sr_x$ $(Zr_{0.5}Ti_{0.5})O_3$ (x = 0.05, 0.10 and 0.15) ceramics. The nature of diffraction pattern shows good homogeneity suggesting the formation of single (perovskite) phase-compounds. The magnified view of peak profile of sample with x = 0.05 in the range of $42 \leq 2\theta \leq 48$ degree is shown in **Fig. 1(b)**. The evolution of two axial reflections (002) and (200) corresponding to a and c axis of tetragonal phase, and (024) reflection corresponds to rhombohedral phase. The existence of reflections in two different systems clearly suggest the coexistence of two phases in the sample of x = 0.05. This assumption on the coexistence of two phases in the sample is very much consistence with recent report on Sr^{2+} doped $Pb(Zr_{0.52}Ti_{0.48})O_3$ [**8**].

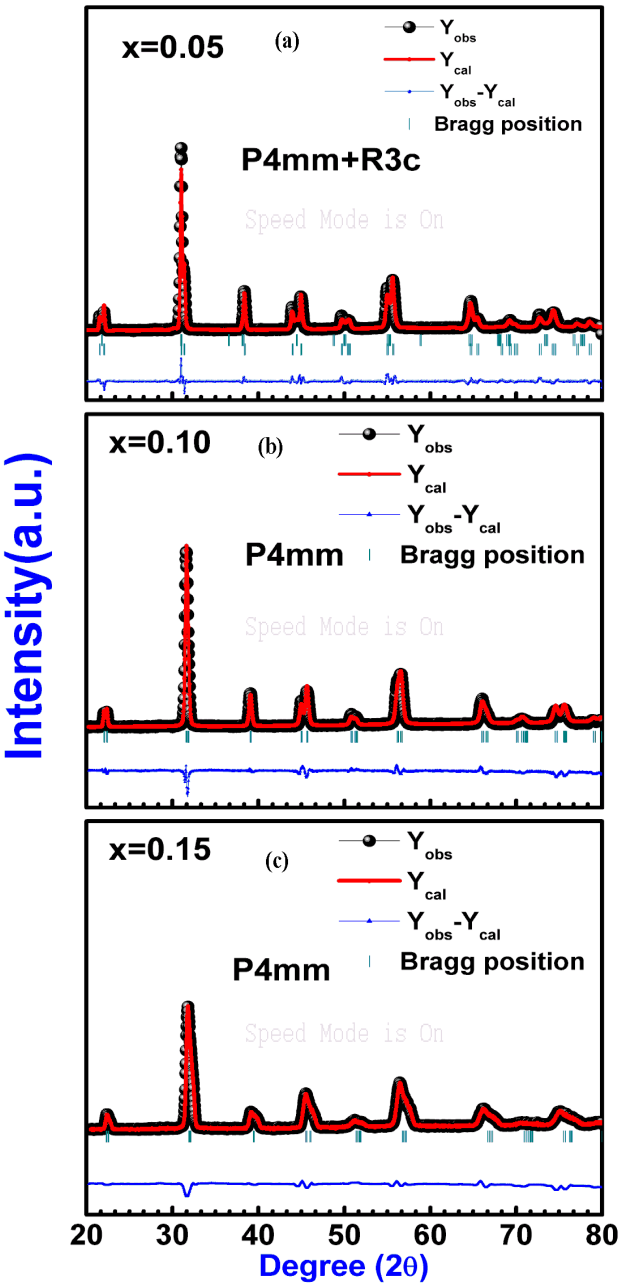

Fig. 2. Rietveld refined X-ray diffraction plots of $Pb_{1-x}Sr_x$ $(Zr_{0.5}Ti_{0.5})O_3$ (x=0.05, 0.10 and 0.15) ceramics.

Furthermore, for the sample with x = 0.10, the reflection (024) get suppressed and /or merges with the broadening of peak. The merging of the rhombohedral peak may be the signature of structural transformation.

To confirm this, careful structural analysis using Rietveld refinement method was carried out. The main results are given below. The initial Rietveld refinement was carried by using zero-point shift unit cell parameters and background points. The shape of reflection profile was modeled using pseudo-Vogt function, and background points were

modelled using linear interpolation between set of background points. During refinement process, some global parameters such as zero-point factor, scale factor, lattice parameter, profile shape parameter, atomic positions etc were varied. The occupancy of all the atoms kept fixed during refinement process [**18**, **19**].

Fig. 2(a-c) shows the experimental and refined XRD patterns for all three samples. **Fig. 2**(**a**) show the Rietveld refined XRD of x = 0.05 composition, where it was well fitted with coexistence of two phases (i.e., (P4mm+R3c)). This result agreed well with the observations made by X-ray diffraction. For, x = 0.1 and 0.15 the XRD data could not be fitted properly with the two-phase model. Therefore, we tried with different space groups such as P4mm, P4/mmm, R3c, C2/m, Pbnm, etc. Among these, the best fit was achieved by the tetragonal with P4mm space group. The magnified view of peak profile of sample with x = 0.10, 0.15 in the range of $42 \leq 2\theta \leq 48$ degree also indicate the presence of pure tetragonal phase. The Rietveld refinement fits between observed and calculated profiles were quite linear with plat profile with acceptable low R-factors. The most important refined parameters (fitting parameters, lattice parameters and R factors) are listed in **Table 1**. As can be seen in **Table 1**, the lattice parameters of $Pb_{1-x}Sr_x(Zr_{0.5}Ti_{05})O_3$ systematically decrease with increasing Sr^{2+} concentration. The decreasing trend in lattice parameter indicates the contraction of unit cell volume, which is due to inclusion of smaller ionic radii an ion (Sr^{2+} (1.44Å)) at the Pb-site [**20**]. From these refinements one can suggests, x = 0.05 sample contain major tetragonal phase with a small fraction of rhombohedral phase. For x = 0.10 and 0.15 samples, single phase with tetragonal (P4mm) crystal structure was observed.

Table 1. Rietveld quantitative phase analysis.

Composition $Pb_{1-x}Sr_x(Zr_{0.5}Ti_{0.5})O_3$	Rhombohederal	Tetragonal	Refinement parameters
x=0.05	a = 5.7529 Å, b = 5.7529 Å, c = 14.1650 Å	a = 4.0279 Å, c = 4.1169 Å	χ^2: 6.05 Rp=16.0
x=0.10	Nil	a = 3.9751 Å, c = 4.0299 Å	χ^2: 4.25 Rp:13.2
x=0.15	Nil	a = 3.9421 Å, c = 3.9862 Å	χ^2: 8.21 Rp:15.1

Microstructural studies

The surface morphology and elemental identification of sintered pellets were carried out by scanning electron microscope. **Fig. 3(a-c)** shows the typical scanning electron microscopy images of the sintered pellet for x = 0.05, 0.10 and 0.15 ceramics respectively. Whereas x=0.05, 0.10 ceramics show well densified grain and grain boundaries, without any significant residual porosity. The observed grains are spherical in shape, which are in the order of 5-10 µm range for x=0.05 and for x = 0.10, it was 1-5 µm range. This observation makes the noted grain size decreases with increasing Sr^{2+} concentrations. The decreasing in grain size with increase of Sr^{2+} concentration is due to substitution of smaller ionic size element/ion (Sr^{2+} (1.44Å)) at the larger ionic size element (Pb^{2+} (1.49Å)) ion. As a consequence of this substitution leads to contract the unit cell volume, as a result, grain size decreases [**20**, **21**]. For x = 0.15 ceramic, the observed grains are more transgranular, it indicates significant stronger internal stresses, which can be larger tetragonal distortion of higher doping of Sr^{2+} doping. These observation reports that the solubility limit of Sr^{2+} in PZT material (perovskite structure) sintered at 1200 ˚C is about 10 mole%. In addition to, nominal compositions of present ceramics were also shown in **Fig. 3(d-e)** as energy dispersive spectra (EDAS). These results suggest our ceramics were pure in phase and compositional homogeneous.

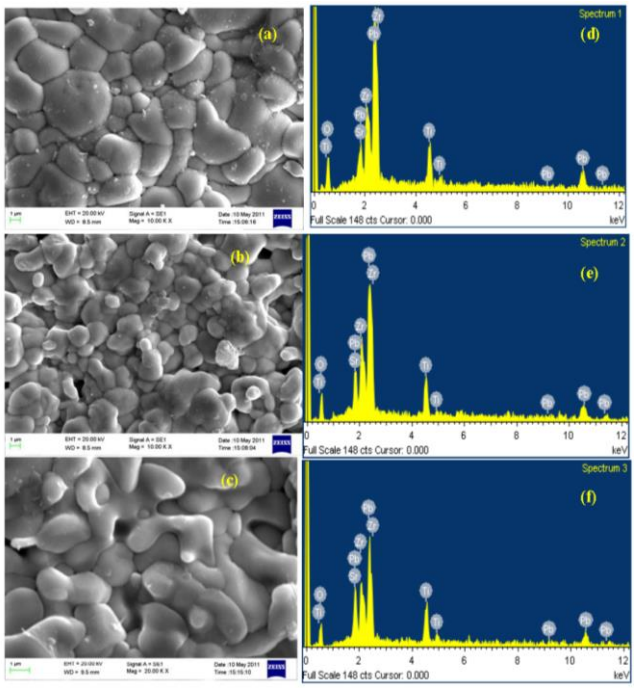

Fig. 3. (a-c) SEM micrographs of the $Pb_{1-x}Sr_x(Zr_{0.5}Ti_{0.5})O_3$ sintered pellets. (a): x=0.05, (b):x=0.10, (c)x=0.15. **Fig.3** (d-f): EDX spectra of the samples.

Dielectric studies

Fig. 4. (a-c) shows the variation of real part of dielectric constant (permittivity) with frequency. The dielectric permittivity decreases with the increase in frequency, and is found to be nearly constant at higher frequencies for all the ceramic samples. For the sample with x = 0.05, it has quite different behavior as compared to others. It can be seen that the sample with x = 0.05 possess high dielectric permittivity at low frequency, even if compared to those of x = 0.10 and 0.15. It is common in the two-phase systems (where oxygen ions in octahedral are loosely bound), that they get distorted by application of an electric field, as a consequence, the value of dielectric permittivity is higher in two-phase systems [**22**]. On the other hand, for higher compositions, at lower frequency the observed dielectric permittivity gets decrease with the increase of Sr^{2+} substitution. The reduction of free charge (defects, oxygen vacancies) carriers on increasing concentration of Sr^{2+} in PZT is possible, as a result, decreases in dielectric permittivity is observed. At higher frequencies, permittivity is found to be nearly constant. The occurrence of this

situation can be understood from the space charge relaxation [**23**]. At low frequencies, the space charges are able to follow the applied field frequency, while, at higher frequencies, they may not have time to undergo relaxation [**24**].

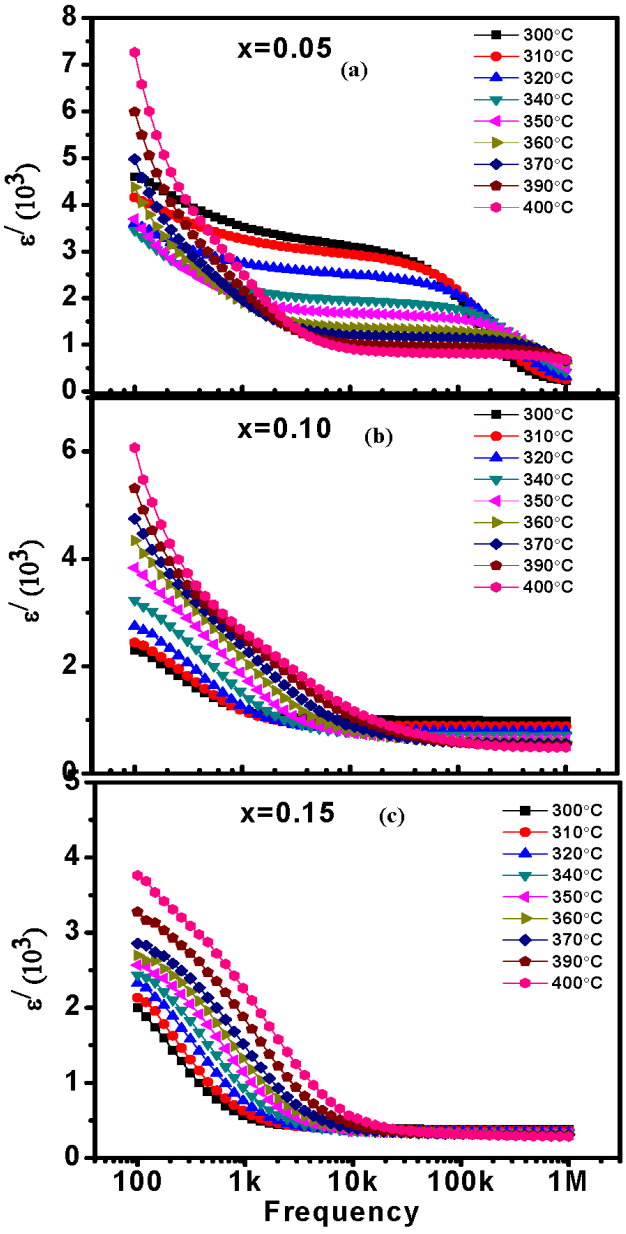

Fig. 4. (**a-c**) Variation of dielectric permittivity with frequency x=0.05, 0.10 and x=0.15 ceramics.

Fig. 5(a-b) shows the temperature-frequency dependence of real and imaginary part of dielectric permittivity for the sample with x=0.05. The two distinct transitions: (in zoomed view was shown inset **Fig. 5(a))** one at ~270 ˚C which is frequency independence and second one is well above (T_m) > 300 ˚C. The frequency independent first transition is known as structural phase transition with the ferroelectric to paraelectric Curie transition (T_C). This conclusion of the present study agrees well with that of $Pb(Zr_{0.5}Ti_{0.5})O_3$ exhibiting Curie temperature of ~ 289˚C [**25**]. Hence, it can be conclude that phase transition at 270˚C of $Pb_{0.95}Sr_{0.05}(Zr_{0.5}Ti_{0.5})O_3$ is associated with the ferroelectric to paraelectric transition. Further, as temperature increases, the real part of dielectric permittivity increases which becomes maximum (T_m), after that it stat decreasing. It was noted that one of common characteristics, T_m (dielectric maxima temperature), is frequency dependent, as expected for a relaxor ferroelectric transition. The large dielectric dispersions are noted below and above T_m in which T_m shifts increasing frequency from 20 kHz–500 kHz. The temperature variation of imaginary part of dielectric permittivity also exhibits similar behavior **(Fig. 5(b))**. The observed dispersion in imaginary component is slightly higher than that of the real part of dielectric permittivity. Therefore, the second transition in the sample with x=0.05 shows diffused-relax or ferroelectric characteristics. Such kind of behavior has also been reported earlier [**26-28**].

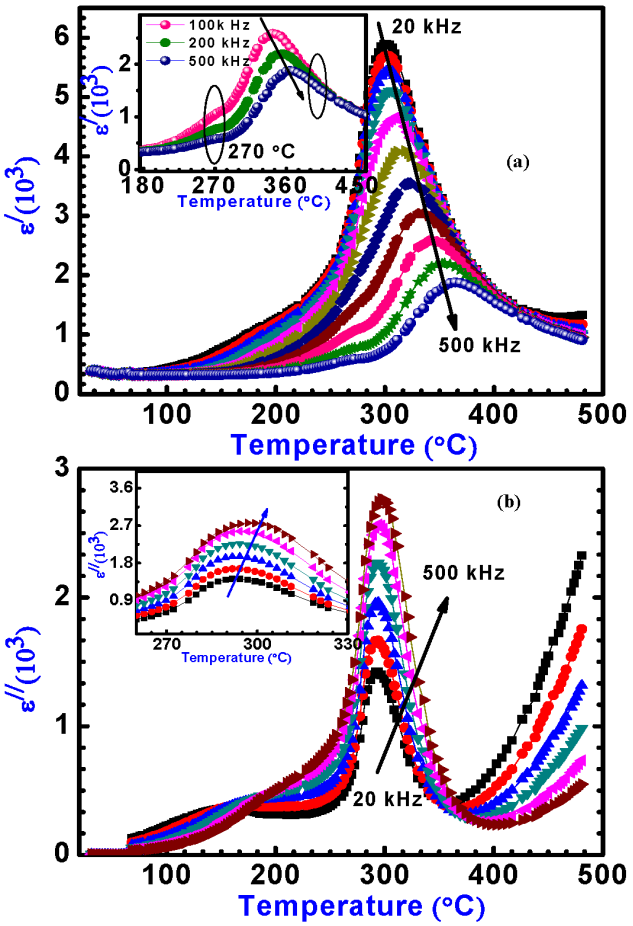

Fig. 5. (a-b) Variation of real and imaginary part of dielectric permittivity with temperature for x=0.05.

On the other hand, occurrence of diffuse phase transition in the material was further confirmed by using Vogul-Fulcher relation and plots. We have plotted T_m with frequency based on Vogul-Fulcher relation **(Fig. 6)**. The Vogul-Fulcher relation; $f = f_o \exp(-Ea/k_B(T_m-T_{VF})$ where f is the measured frequency, f_0 is a pre exponential function, E_a is activation energy, k_B is the Boltzmann constant, T_m is the temperature corresponding to the dielectric maxima, and T_{VF} is the characteristic Vogel–Fulcher freezing temperature explains a freezing process of the polar nano-regions (PNRs) [**29**, **30**]. The fitted parameters **(Fig.6)**

agree well with the reported ones [**31**]. At certain nonzero temperature, thermal motion capable of destroying the ordered oxygen sites may create polar nano-regions inside the grains. Such orderly arranged PNRs can act as unusually large dipoles which are always frequency dependent on application of external electric field [**31**].

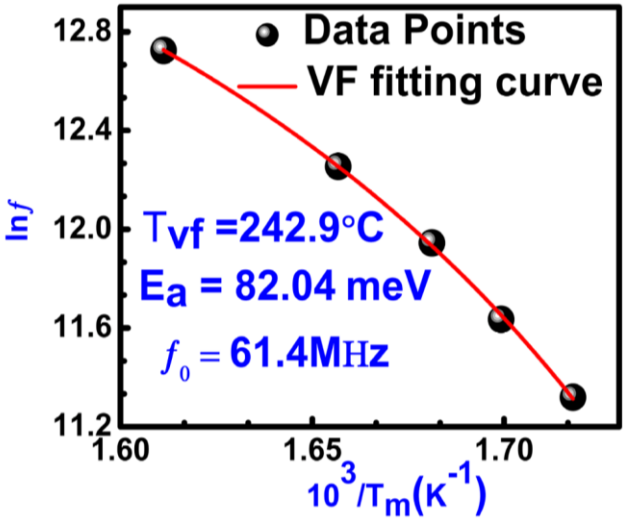

Fig. 6. Variation of lnf v/s 10^3/T with Vogul-Fulcher fitting curve for x=0.05 ceramic.

Fig. 7(a-b) shows the temperature dependence of real and imaginary component of complex dielectric permittivity at fixed frequencies for samples of PSZT (with x=0.10 and 0.15). On increasing Sr^{2+} content in PSZT, the room temperature real part of dielectric permittivity increases. The observed values of real component are 445, 1112, and 1431 for the PSZT samples with *x*=0.05 0.10, and 0.15 at 20 kHz respectively. Moreover, the frequency independence of permittivity maxima, (similar to the normal paraelectric to ferroelectric transition) was noted for PSZT of x=0.10 and 0.15. The observed Curie (T_C) transition is 198˚C for x=0.10 and 100˚C for x=0.15. The shifting of T_C towards lower temperature as function of increasing Sr^{2+} concentration in PZT was observed. The decreasing in T_c towards lower temperature can be explained on the nature of bond and ionic radii of A and B-site atoms of perovskite systems. In the ABO_3-type ferroelectrics, the ferroelectric characteristics are obtained by balancing the long-range coulomb interaction and short-range force. The long range coulomb interaction is associated with the effective transfer of charges at the B-site. As the charges increase at the B-site, the attractive coulomb potentials increase at this site [**32**]. The increasing transferred charges might induce strong splitting of the ferroelectric modes between longitudinal optical and transverse optical. In the present case, partial substitution of A-cation (Pb^{2+} by Sr^{2+}) decreases the number of unoccupied O (2p)-Ti/Zr (3d) hybridization states. It is due to large separation of electro-negativity between Sr^{2+} and Pb^{2+}, (electro-negativity (Sr^{2+}) < electro-negativity (Pb^{2+})). Its effective charge is likely to be decreased, when Pb^{2+} is replaced with Sr^{2+}. Thus, this reduction of effective charge on Ti/Zr site decreases the Coulomb force between O (2p) and Ti/Zr (3d). As a consequence, the longitudinal optical (LO)- transverse optical (TO) splitting might be reduced.

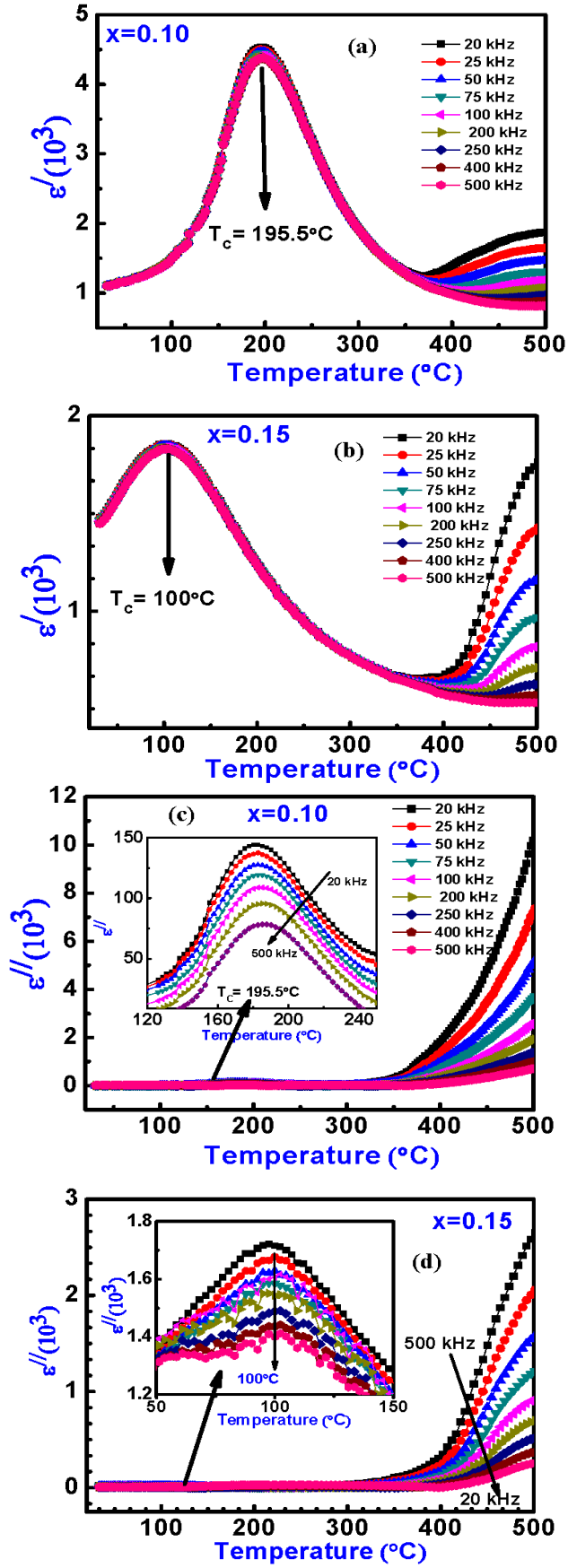

Fig. 7 (a-b) Real part of dielectric permittivity with temperature for x=0.10 and 0.15 ceramics, (c-d) variation of imaginary part of dielectric permittivity with temperature at fixed frequencies.

The decrease of LO-TO splitting can shift the ferroelectric nature towards room temperature. Therefore, the expected phase transition temperatures are shifted towards lower values in $Pb_{1-x}Sr_x(Zr_{0.5}Ti_{0.5})O_3$ on increasing Sr^{2+} concentration in PSZT.

Fig. 7 (c-d) shows the temperature variation of imaginary part of dielectric permittivity of PSZT samples (x=0.10 and 0.15). The tangent loss in these compounds was found to be in the order of 0.01 to 0.1 at room temperature. These values agreed with those of reported ones. The imaginary component also has the same Curie temperature, as observed in the real part of dielectric permittivity. From these studies one can conclude that even small content of Sr^{2+} in PSZT leads to the large decrease in Curie transition.

Impedance studies

Complex impedance spectroscopy is an effective method to extract information related to bulk (grains), grain boundaries and electrode-material interface by conjunction with simple impedance formulation. Besides this, it enables us to estimate the relaxation frequency (f_{max}), which is an intrinsic property of the material, independent of its geometrical factors. **Fig. 8**(**a-c**) shows the variation of Z' v/s *Z*" (Nyquist plots) at temperature 400˚C below and above. The presence of more than one type of relaxation process can be seen from the nature of curves. In case of lower concentration of Sr (x=0.05 and 0.10), a proposed circuit model of three parallel RC combinations of (R_g, CPE C_g), (R_{gb}, C_{gb}) and (R_{int}, C_{int}) was found to have excellent agreement (solid line) with that of experimental data (solid dot) for the materials (**Fig. 8(a-b)** with inset). In addition to, a constant phase factor (CPE) was introduced in place of grain capacitance on each ceramic. It is known that the impedance of CPE can be expressed as: $Z_{CPE} = \frac{1}{A}(j\omega)^{-n}$ here ω is angular frequency, n is relaxation time distribution function and A is a constant. For Debye type relaxation, α has the value of unity whereas the non Debye type relaxation processes the n value in the range of $0 \leq n \leq 1$. From the observed value of n, one can easily conclude that non Debye type relaxation dominates in all ceramics.

The observed values of resistance and capacitance of grain, grain boundary and interface decrease with increasing temperature indicating the semiconductor nature of the ceramics. It is also observed that with increasing Sr^{2+} concentration, the contribution from the grain boundary resistance dominants, and interfacial polarization become negligible. This modification can be clearly shown in **Fig. 8(c),** while data was well fitted with two parallel RC combinations of (R_g, CPE, C_g), (R_{gb}, C_{gb}). The significant change in grain and grain boundary electrical properties of the samples may be attributed to charge ordering within the sample matrix on increasing concentration of Sr^{2+} of PZT.

Fig. 9 (a-f) shows the variation of imaginary component of complex impedance as a function of temperature and frequency range. It is observed that all the samples display two broad peaks at low frequency (10 kHz) and intermediate frequency (≤ 100 k Hz) respectively. Beside this, the peak maxima shift towards higher frequency on increasing temperature, and these curves merge at and above 100 kHz. It is evident from Nyquist plots that multiple relaxation times and processes are associated with grain, grain boundaries and interfacial. The multiple broad dielectric relaxations is interrelated to various factors including size-distribution, wall-motion and orientation of domains, defect dipoles created causing diffuse dielectric transitions.

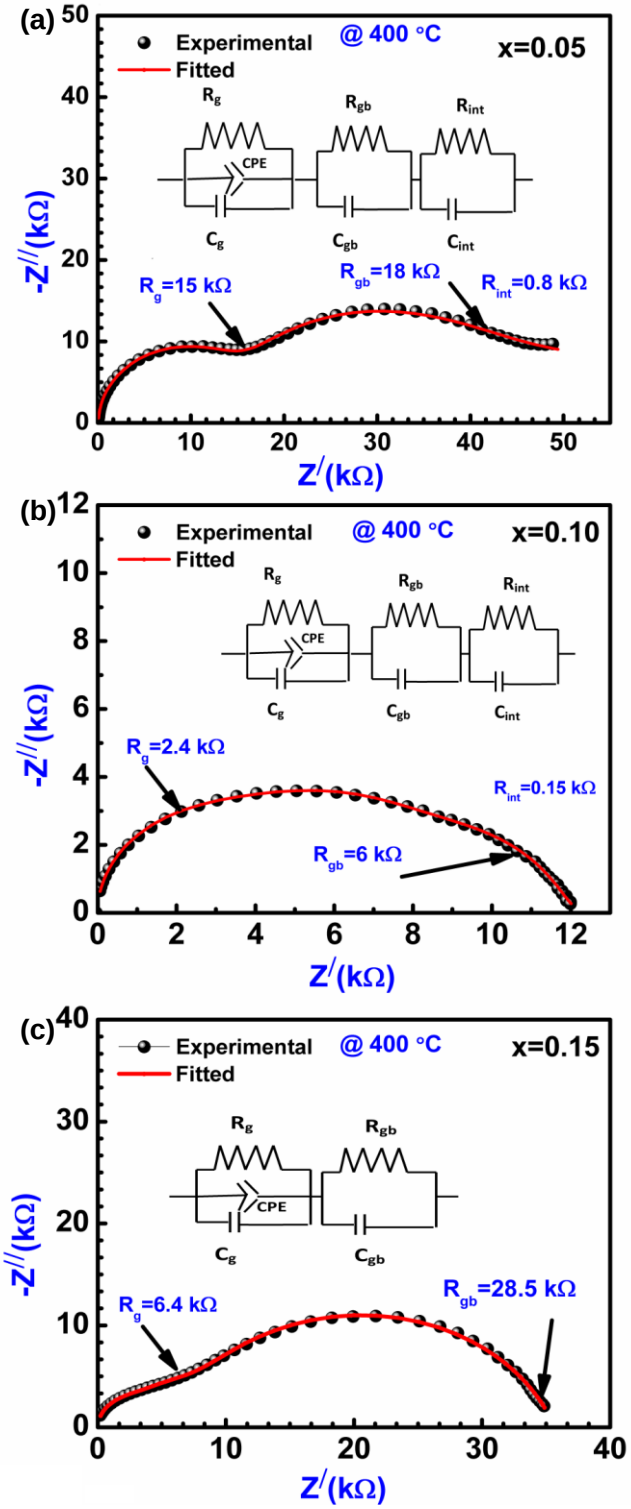

Fig. 8. Complex (Nyquist plots) for x=0.05, 0.10 and x=0.15 at 400˚C temperature.

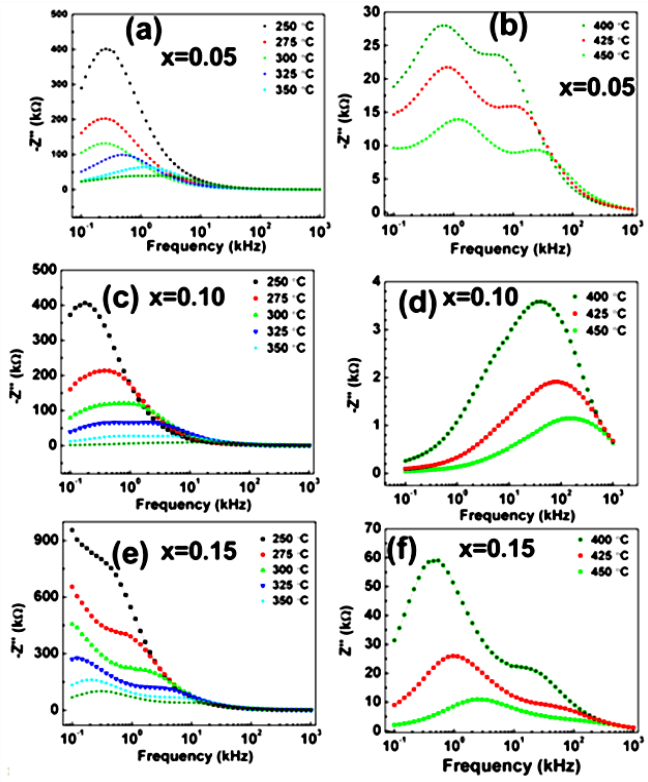

Fig. 9. Frequency dependent of imaginary part of impedance (Z") for x=0.05, 0.10 and x=0.15 at different temperature.

The activation energy associated with each peak was calculated using resonance condition $\omega\tau=1$ (angular frequency) and equation $f = f_o\exp(-E_a/k_BT)$. where $f_o$is a pre-exponential factor, k and T have their usual meaning. The observed relaxation frequency associated to these ceramics strictly follows Arrhenius law. Relaxation associated to each peak is plotted as ln(f) v/s 10^3/T is shown in **Fig 10**. The noted activation energies are of 0.48 eV, 0.34 and 0.31 eV corresponding to x=0.05, 0.10 and 0.15 respectively. These values are consistent with the activation energy corresponds to charge hopping between grain and grain boundary regions.

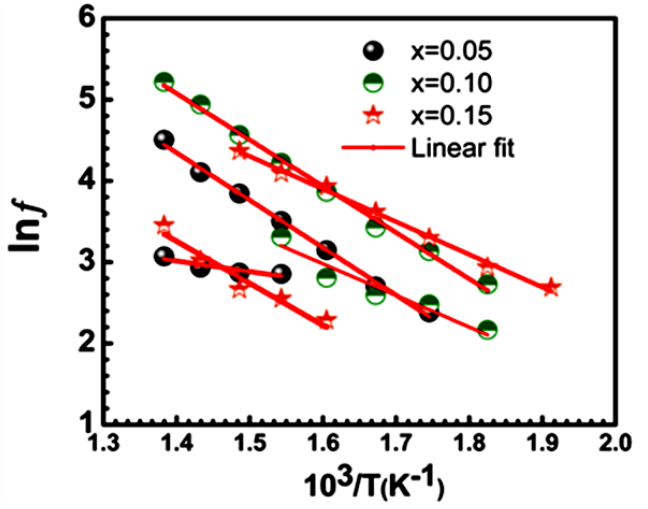

Fig. 10. Temperature dependence of lnf v/s 10^3/T obtained from Z" curves. (solid red curve is Arrhenius law fitted curve)

Conclusion

In summary, it has been shown that the present ceramics were successfully synthesized by a conventional high-temperature solid-state reaction technique. The Rietveld refined parameters and XRD profile (at room temperature) showed the coexistence of two phases i.e., (P4mm+R3c) tetragonal and rhombohedral phase for $Pb_{0.95}Sr_{0.05}(Zr_{0.5}Ti_{0.5})O_3$ ceramic and for higher concentration of $Sr^{2+,}$ material was found in the tetragonal phase with space group P4mm. It is also shown that the grain size in PSZT decreases with increasing Sr^{2+} concentrations because of substitution of smaller ion (radii of Sr^{2+}) at larger ions Pb^{2+}. The temperature and frequency dependence of real/imaginary components of complex dielectric permittivity of PSZT showed the large change in Curie temperature as a function of Sr^{2+} ascribing a large separation of electro-negativity between Sr^{2+} and Pb^{2+}, leads to reduces effective charge on B - site. The effective charge transfer reduction can decrease the ferroelectric LO-TO splitting as a result reduced Curie temperature was observed. It also shown from Nyquist plots that multiple relaxation times and processes associated with grain, grain boundaries and interfacial polarization for x=0.05, x=0.10 and grain boundary conduction found to be dominant for x=0.15. To study such divalent (Sr^{2+}, Ca^{2+}, Ba^{2+}) doped PZT near to MPB leads to interested modulation in enhancing in physics properties. To understand such materials physical properties will be useful for future piezoelectric sensors, infrared detectors, medical imaging, and future piezoelectric transformers.

Acknowledgements

For financial support, authors Nawnit Kumar and Mukul Pastor express thanks to CSIR, New Delhi, India and Dr D.S. Kothari fellowship (Grant no. F.4-2/2006(BSR)/13-360/2010(BSR)).

References

1. Spearing, S. M., *Acta Mater.* **2000**, *48*, 179. **DOI**: 10.1016/S1359-6454(99)00294-3
2. Cross, L. E., *Jpn. J. Appl. Phys.* **1995**, *34*, 2525. **DOI:** 10.1143/JJAP.34.2525
3. Raymond, O., Font, R., Suarez-Almodovar, N., Portelles, J., Siqueiros, M., *J. Appl. Phys.* **2005**, *97*, 084108. **DOI**: 10.1063/1.1870099
4. Viehland, D., *Phys. Rev. B* **1995**, *52*, 778. **DOI:** 10.1103/PhysRevB.52.778
5. Zhang, S., Li, F., *Jpn. J. Appl. Phys.* **2012,** *111*, 031301-1. **DOI:** 10.1063/1.3679521
6. Uchino, *Solid State Ionics* **1998**, *108*, 43. **DOI:** 10.1016/S0167-2738(98)00017-4
7. Moulson, A. J.; Herbert, J. M., *Electroceramic Material. Properties: Applications* (Chapman and Hall, New York, 1990).K. **DOI:** 10: 0412294907
8. Bedoya, C.; Ch. Muller b, Baudour, J. L.; Madigou, V.; Anne, M.; Roubin, M., *Material. Sci. Engg. B* **2000**, *75*, 43. **DOI:** 10.1016/S0921-5107(00)00383-4
9. Prabu, M.; Shameem Banu, I. B.; Gobalakrishnan, S.; Chavali, M., *J. Alloy. Compnd.* **2013**, 551, 200. **DOI**:10.1016/j.jallcom.2012.09.095
10. Zeng, X.; He, X.; Cheng, W.; Zheng, X.; Qiu, P., *J. Alloy. Compnd.* **2009**, *485*, 843. **DOI**: 10.1016/j.jallcom.2009.06.106
11. Raman, K.; Lopez, M., *J. Alloys Compd.* **2008**, *466*, 398. **DOI:** 10.1016/j.jallcom.2007.11.055
12. Ranjan, R.; Kumar, R.; Kumar, N.; Behera, B.; Choudhary, R. N. P., *J. Alloys Compd.* **2011**, *509*, 6388. **DOI**:10.1016/j.jallcom.2011.03.003

13. Shannigrahi, S. R.; Tay, F. E. H.; Yao, K.; Choudhary, R. N. P.; *J. Eur. Ceram. Soc.* **2004**, *24*, 163. **DOI:** 10.1016/S0955-2219(03)00316-9
14. Zheng, H.; Reaney, I. M.; Lee, W. E.; Jones, N.; Thomas, H., *J. Eur. Ceram. Soc.* **2001**, *21*, 1371. **DOI**: 10.1016/S0955-2219(01)00021-8
15. Nasar, R. S.; Cerqueira, M.; Longo, E.; Varela, J. A.; Beltran,A., *J. Eur. Ceram. Soc.* **2009**, *22*, 209. **DOI**: 10.1016/S0955-2219(01)00256-4
16. Kalem, V.; Cam, I.; Timucin, M.; *Ceramic. Inter.* **2011**, *37*, 1265. **DOI**: 10.1016/j.ceramint.2010.12.003
17. Kumar, N.; Tirupathi, P.; Kumar, B.; Pastor, M.; Pandey, A. C.; Choudhary, R. N. P., *Adv. Mat. Lett.* **2015**, *6*, 284. **DOI:** 10.5185/amlett.2015.6618
18. Palatinus, L.; Chapuis, G., *J. Appl. Crystal* **2007**, *40*, 786. **DOI**:10.1107/S0021889807029238
19. McCusker, L. B.; Von Dreele, R. B.; Cox, D. E.; Louer, D.; Scardi, P., *J. Appl. Crystal* **1999**, *32*, 36. **DOI**: 10.1107/S0021889898009856
20. Pandey, S. K.; Thakur, O. P.; Bhattacharya, D. K.; Chandra Prakash, Chatterjee, R., *J. Allys. Compnd.* **2009**, *468*, 356. **DOI:** 10.1016/j.jallcom.2008.01.006
21. Dutta, S.; Choudhary, R. N. P., *Appl. Phys. A*., **2008**, *90*, 323. **DOI:** 10.1007/s000339-007-4276-2
22. Gerber, P.; Bottger, U.; Waser, R., *J. Appl. Phys.* **2006**, *100*, 124105. **DOI:** 10.1063/1.2401047
23. Pradhan, S. K.; Roul, B. K.; *J. Phys. Chem. Solids* **2011**, *72*, 1180. **DOI**: 10.1016/j.jpcs.2011.07.017
24. Wang, Y.; Shao, Q. Y.; Liu, J. M.; *App. Phys. Lett.* **2006**, 88, 122902. **DOI:** 10.1063/1.2188591
25. Leech, P. W.; Holland, A. S.; Sriram, S.; Bhaskaran, M., *App. Phys. A*, **2008**, *91*, 679. **DOI:** 10.1007/s000339-017-9350-6
26. Guo, Y.; Luo, H.; He, T.; *Mater. Res. Bull.* **2003**, 38, 1501. **DOI**: 10.1016/S0025-5408(03)00177-6
27. Shrout, T. R.; Chang, Z. P.; Kim, N.; Markgraf, S.; *Ferroelectr. Lett. Sect.* **1990**, *12*, 63. **DOI:** 10.1080/07315179008201118
28. Vittayakorn, N.; Rujijanagul, G.; Tan, X.; A. Marquardt, M.; P. Cann, D., *J. Appl.Phys.* **2004**, *96*, 5103. **DOI:** 10.1063/1.1796511
29. Mulvihill, M. L.; Cross, L. E.; Cao, W.; Uchino, K.; *J. Am. Ceram. Soc.* **1997**, *80*, 1462. **DOI:** 10.1111/j.1151-2916.1997.tb03004.x
30. Cheng, Z. X.; Wang, X. L.; Alvarez, G.; Dou, S. X.; Zhang, S. J.; *J. Appl. Phys.* **2009**, *105*, 07D902. **DOI:** 10.1063/1.3055266
31. Pirc, R.; Blinc, R., *Phys. Rev. B* **2007**, *76*, 020101. **DOI:** 10.1103/PhysRevB.76.020101
32. Bokov, A. A.; Ye, Z. G., *J. Mat. Scen.* **2006**, *41*, 52. **DOI:** 10.1007/s10853-005-5915-7

